Single-Layer Fishbone-Shaped Frequency Selective Surface with Stable Performance

Mantang Cui*, Yangyi Lu, Hong Yuan, and Suyang Shi

Abstract—A novel single-layer band-pass frequency selective surface (FSS) is proposed in this letter. The unit cell is composed of eight rotationally symmetrical fishbone-shaped structures surrounded by a modified octagonal loop. This fishbone-shaped FSS exhibits stable resonant frequency while the incident angle ranges from $0°$ to $60°$ for both TE and TM polarizations, which means that polarization insensitivity and angular stability are well demonstrated on the proposed FSS. A prototype is fabricated and measured in an anechoic chamber, and good agreements are obtained between measured and simulated results.

1. INTRODUCTION

Frequency selective surfaces (FSSs) can be viewed as generalized spatial filters with band-stop or band-pass characteristics. So far, FSSs have found a wide range of applications from low microwave to terahertz and optical frequency [1], and due to its versatility, FSSs have been extensively used as antenna radomes [2], microwave EMI shielding [3], polarization convertors [4], absorbers [5], metasurfaces [6], etc.

However, many engineering applications (such as radar radomes or aircraft stealth) strictly require that the frequency selection characteristics cannot be deteriorated with changes in the incident angles and polarizations of electromagnetic wave [7]. Traditional FSSs could not meet these high requirements, so new forms of FSSs with good angular stability and polarization insensitivity have attracted much more attentions in recent years. Many attempts have been made to enhance the stability of FSSs, and generally an effective approach is to design miniaturized and symmetrical structures [8, 9].

The method in [10] proposes an ultra-miniaturized FSS unit cell by loading lumped components to produce a resonant loop similar to that found in band-pass aperture. The unit size is less than $\lambda_0/100$, where λ_0 is the resonant wavelength in free space, and the transmission performance for both TE and TM polarizations is stable even the oblique incident angle is up to $75°$. However, the operating bandwidth of the loaded FSS is relatively narrow, and the tolerance of the lumped components makes it a challenge to maintain a stable resonance performance.

The convoluted structure is a direct method to achieve miniaturization, and many existing curl designs have thin and long microstrip lines arranged on single-layer printed board. For these compact FSSs, it is impossible to design a long enough convoluted strip line on the limited unit area due to the limitations of the PCB process. Multilayer technique is a good choice to solve it. In [11], a method of adding metallic vias on multi-layered convoluted elements is mentioned to realize a miniaturized FSS. The size of unit cell can be reduced to $0.033\lambda_0 \times 0.033\lambda_0$, and a great stable angular response up to $75°$ is achieved. Nevertheless, the higher processing accuracy and manufacturing cost need to be considered for these multilayer FSSs with metal vias.

Compared with the planar FSS, 3D FSS has gained more research interest recently owing to its multi-mode, broadband, and sharp filtering response [12–14]. The unit cell of the 3D FSS in [14] consists of an array of three-layer parallel strip lines with inserted metallic rods and two identical single-layer patch arrays. The 3D structure exhibits stable dual-band performance with arbitrary band ratios under a variation of incident angles from 0° to 40°. Despite its good properties, the thickness of the unit cell is $0.083\lambda_0$, which may limit its practical application.

In this letter, a novel fishbone-shaped band-pass FSS is put forward, and a group of rotationally symmetrical fishbone-shaped structures are designed on a single-layered printed board. Thus, the proposed FSS has the advantages of easy processing, low profile, and beautiful appearance. Moreover, the simulated results show that it has good stability with respect to different polarizations and incident angles. The FSS is manufactured and tested, and the measured transmission curves have good consistency with the simulation.

2. DESIGN PROCEDURE AND ANALYSIS

The unit cell geometry of the proposed FSS is shown in Figure 1. The design procedure can be divided into four steps. Firstly, the basic FSS model (BFS) of a rectangular patch with an octagonal loop is designed, as shown in Figure 1(a). Secondly, eight rotationally symmetrical tapered slots are etched on the inner octagonal metal surface of the basic FSS model (TBFS in Figure 1(b)). The edge line of a tapered slot is an exponential gradient line satisfying the formula $y = c_1 e^{\alpha x} + c_2$. Then, a group of five small rectangular slots is etched symmetrically in each of the four corners of the rectangular patch (RTBFS in Figure 1(c)). Finally, a set of concentric circular slots are embedded on the inner frame, and the final fishbone-shaped geometry is obtained, which is shown in Figure 1(d).
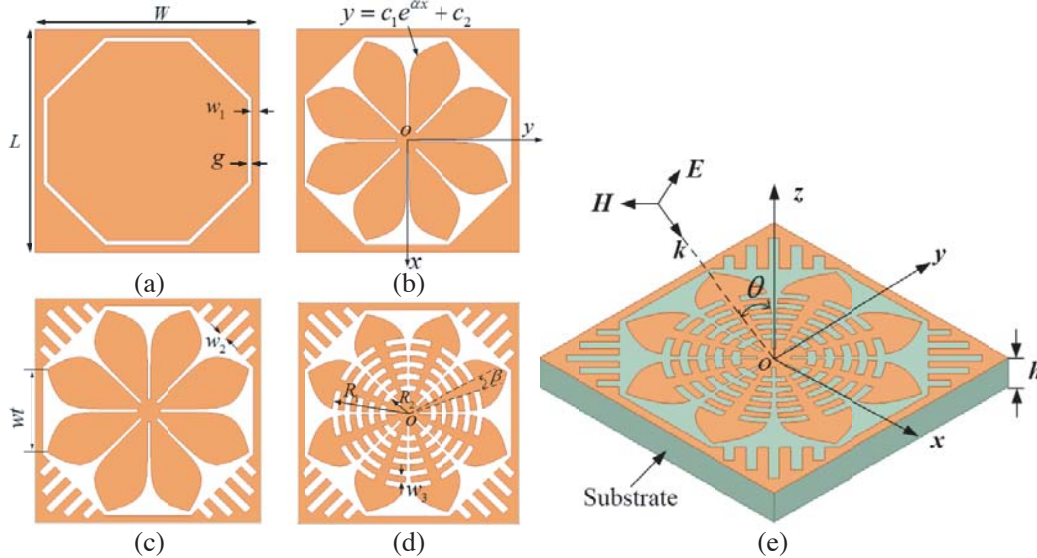

Figure 1. Design procedure: (a) BFS, (b) TBFS, (c) RTBFS, (d) the final fishbone-shaped geometry and (e) the proposed FSS model.

The designed FSS structure is printed on a Rogers RO5880 substrate with the relative permittivity of 2.55 and loss tangent of 0.002. The complete FSS unit model is shown in Figure 1(e), and the full dimension $W \times L$ is 15 mm × 15 mm, the thickness h is 1.524 mm. Other geometric dimensions of the model are: $wt = 5.5$ mm, $w_1 = 0.5$ mm, $w_2 = 0.5$ mm, $w_3 = 0.4$ mm, $R_1 = 5.1$ mm, $R_2 = 1.5$ mm, $g = 0.3$ mm, $\gamma = 18°$.

For the FSS structures in Figure 1, the equivalent circuit models are shown in Figure 2(a). The basic FSS structure in Figure 1(a) can be equivalent to an LC parallel circuit with a resonance of $f = 1/(2\pi\sqrt{LC})$. The proposed FSS structure etching a series of slots on the surface metal in Figure 1(d)
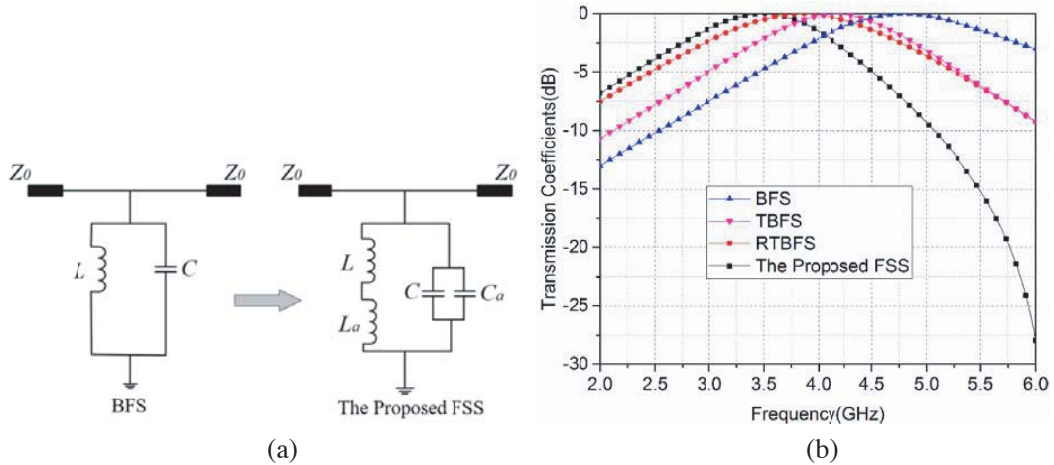
Figure 2. (a) Equivalent circuit model and (b) transmission coefficients of different structures.

is equivalent to adding extra capacitance C_a and inductance L_a to the basic circuit model [15], and the resonant frequency can be expressed as $f = 1/(2\pi\sqrt{(L + L_a)(C + C_a)})$. From the analysis of the equivalent circuit, the resonance will be reduced due to the additional capacitance and inductance, which is conductive to the realization of miniaturization.

The transmission coefficients of the BFS, TBFS, RTBFS, and the proposed fishbone-shaped FSS at normal incidence are simulated using commercial software ANSYS HFSS, and the results are presented in Figure 2(b). The resonances are obtained at 4.79 GHz, 4.17 GHz, 3.86 GHz, and 3.5 GHz corresponding to the four FSS structures shown in Figures 1(a)–(d). Therefore, compared with the basic FSS model, the tapered slots, rectangular slots, and circular slots in the proposed design can obviously lower the resonant frequency of the passband. This conclusion is consistent with the analysis of the equivalent circuit model.

The proposed FSS model is researched for different polarization angles from 0° to 90° under normal incident wave, and it can be observed that similar transmission responses for all angles are shown in Figure 3, which proves the designed FSS polarization-insensitive. Besides, the -3 dB bandwidth is 1.61 GHz ($2.64 \sim 4.25$ GHz), and -1 dB bandwidth is 0.86 GHz ($3.04 \sim 3.9$ GHz), while the fractional bandwidths are approximately 46% and 24%, respectively. It indicates that the proposed structure has good transmission characteristics at a wide frequency band.

To further investigate the stable performance, the designed FSS is analyzed in different incident angles ranged from 0° to 60° for both TE and TM polarizations. The transmission coefficients are
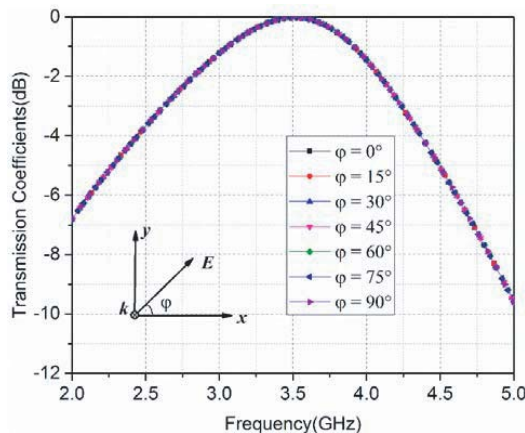

Figure 3. Transmission coefficients of the proposed FSS for different polarization angles.
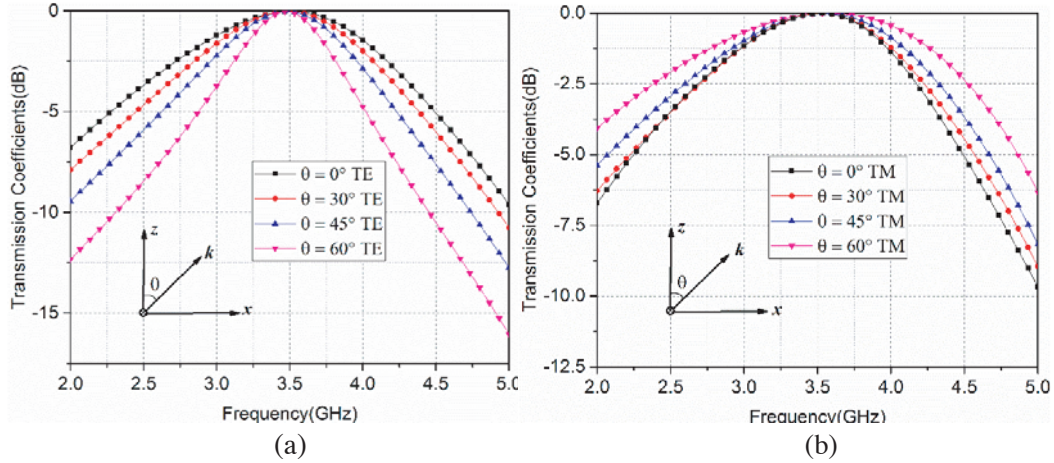
Figure 4. Transmission coefficients of the proposed FSS under different incident angles with (a) TE polarization, (b) TM polarization.

shown in Figure 4, and it can be seen that for both TE and TM polarizations, the resonance frequency is well maintained at 0°, 30°, 45°, and 60° incident angles, and the maximum frequency deviations are less than 20 MHz for TE polarization and 70 MHz for TM polarization. So, the proposed FSS exhibits good angular stability property at large incident angles. Meanwhile, the same analysis has also been performed on the BFS, TBFS, RTBFS structures shown in the design procedure, and Table 1 gives the comparison of stable performance. As shown, within the incident range of 0 to 60 degrees, the maximum frequency deviation of BFS is as high as 5%, and after the fish-bones shaped design on BFS model, the enhanced angular stability is obtained due to the maximum deviation of the proposed FSS of only 2%.

Table 1. Comparison of the stable performance of all FSS structures.

FSS	Resonant Frequency (GHz)	Max deviation (GHz) (0 ~ 60°)		Max deviation percentage
		TE	TM	
BFS	4.79	0.16	0.24	5%
TBFS	4.17	0.03	0.15	3.6%
RTBFS	3.86	0.02	0.10	2.6%
The Proposed FSS	**3.5**	**0.02**	**0.07**	**2%**

Furthermore, it is worth noting that when the incident angle is 60 degrees for TE polarization, the 3 dB fractional bandwidth of the single-layer slotted metal FSS in the reference [7] is only 14%, while it can reach 23% for the proposed single-layer dielectric FSS in this letter. This can demonstrate an improvement in bandwidth compared with the traditional band-pass element for a single-layer FSS.

To clarify the mechanism of the polarization insensitivity and angular stability, the current distribution on the surface of the proposed FSS is depicted at the resonance frequency 3.5 GHz. It can be seen in Figure 5 that at normal incidence, the current generated by TE polarized wave is mainly distributed on the fishbone structures numbered 2, 3, 6, and 7 (Figure 5(a)), while the current corresponding to TM polarized wave is distributed on 1, 4, 5, and 8 (Figure 5(b)). The current distributions in the two cases are almost the same, and combined with the rotational symmetry of the fishbone structure, it can well illustrate the stable performance of polarization insensitivity. In addition, when the incident angle reaches 60°, the current distribution generated by TE (Figure 5(c)) and TM polarizations (Figure 5(d)) is very similar to that of normal incidence, which indicates that the
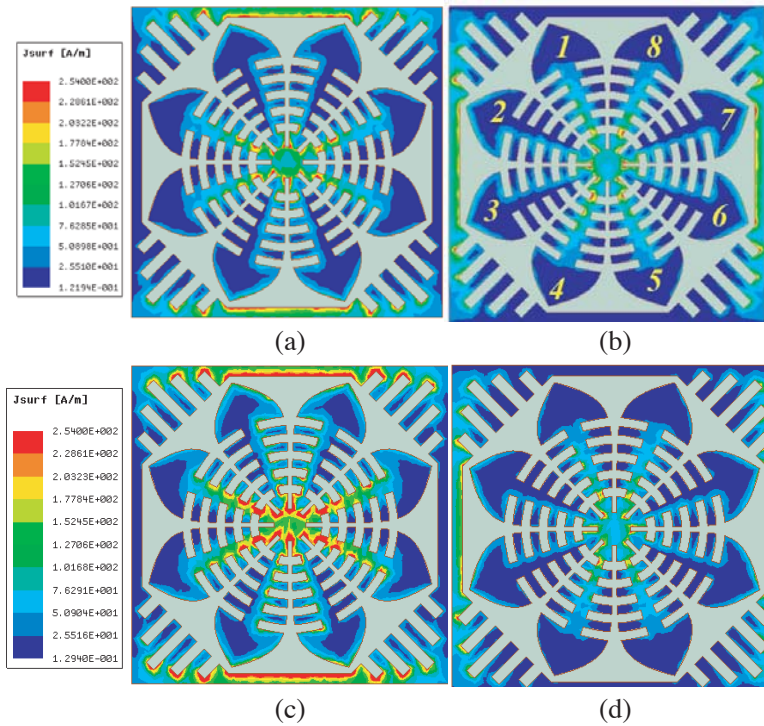
Figure 5. Current distribution at normal incidence with (a) TE polarization, (b) TM polarization and incident angle of 60° with (c) TE polarization, (d) TM polarization.

designed FSS has the characteristic of angular stability.

In the design process, the resonance frequency changes with the size of the tapered slot, and especially the opening size wt has a significant effect on it. In Figure 6(a), the transmission coefficients of the FSS with different values of wt are given. As the values vary from 2 mm to 6.5 mm, the corresponding resonant frequency decreases from 3.65 GHz to 3.1 GHz. Moreover, the change of the gradient index α of the tapered edge line will also affect the resonance. As shown in Figure 6(b), when the value of α increases, the resonance will decrease accordingly.
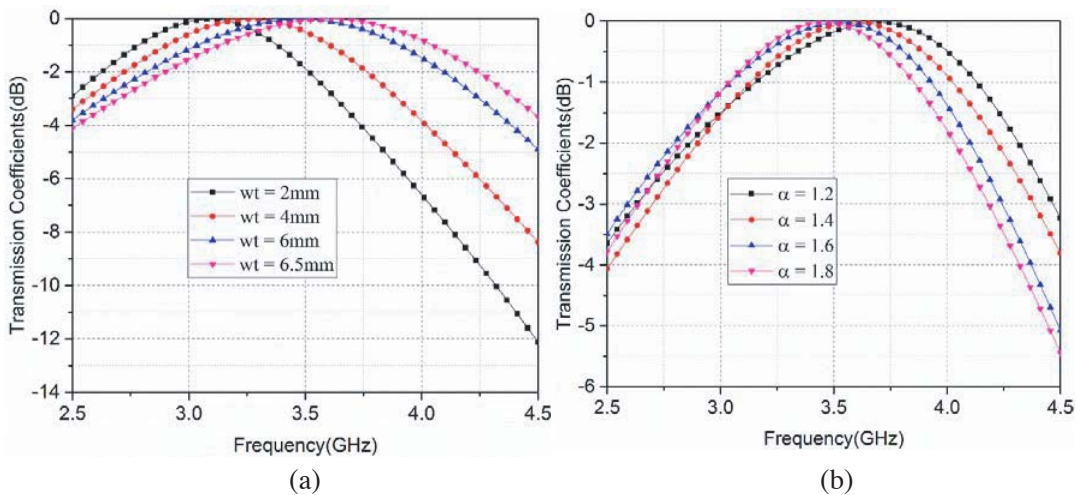

Figure 6. Comparisons of different values of variables (a) wt and (b) α.

3. EXPERIMENTAL VERIFICATION

To verify the simulated performance, a prototype of the proposed fishbone-shaped FSS is manufactured and measured. Figure 7(a) shows the fabricated structure containing 10×10 unit cells, and the oversize is $150 \times 150\,\text{mm}^2$. The experiment has been carried out using the free-space method in an anechoic chamber, and a pair of transmitting and receiving antennas are connected to an Anritsu 37247D vector network analyzer (VNA) as explained in Figure 7(b). The transmission coefficients at incident angles of $0°$, $30°$, $45°$, and $60°$ for both TE and TM polarizations are tested, and the results are shown in Figure 7(c) and Figure 7(d). It can be concluded that the measured curve is in good agreement with simulated results, and the resonance frequency remains the same with different incident angles and polarizations, which proves that the proposed FSS has stable performance. The little difference can be attributed to the influence of the edge diffraction.
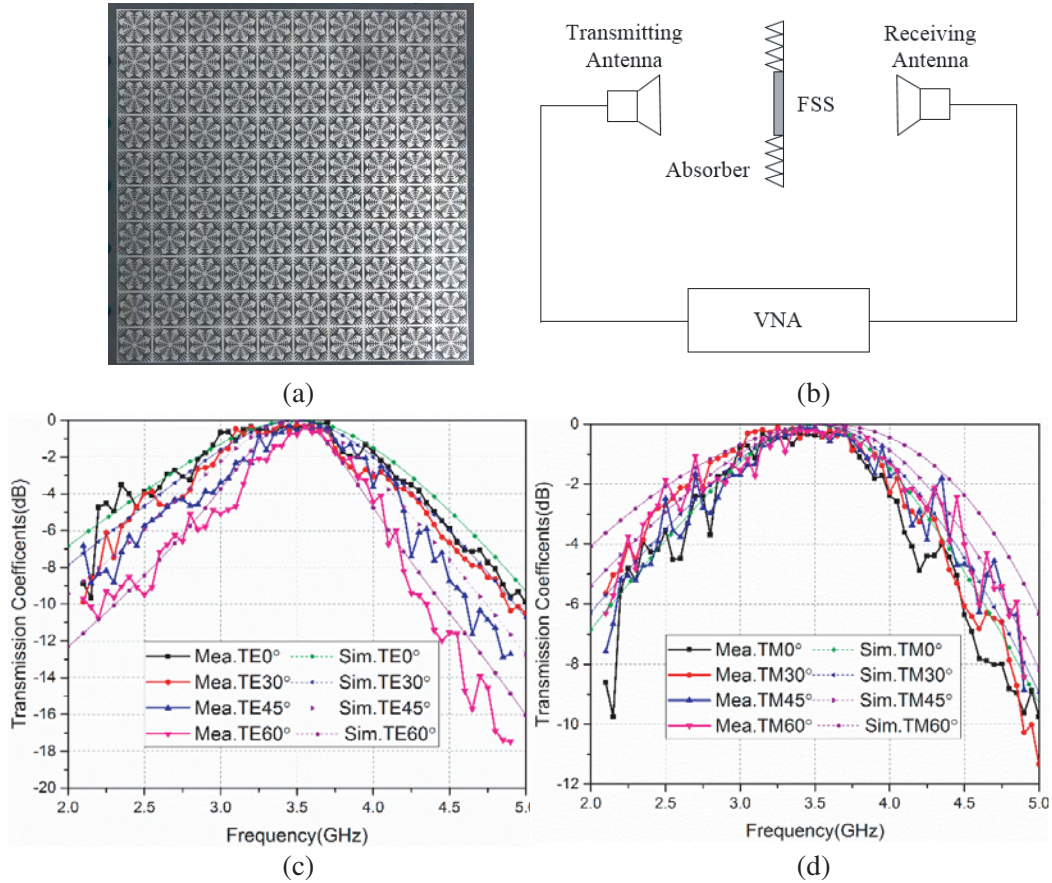

Figure 7. (a) Fabricated structure, (b) measurement setup, measured and simulated results for (c) TE polarization and (d) TM polarization.

4. CONCLUSION

In this letter, a novel single-layer fishbone-shaped FSS with bandpass characteristics is presented. For both TE and TM polarizations, the proposed FSS exhibits stable behavior of polarization insensitivity and angular stability when the incident angle ranges from $0°$ to $60°$. In addition, the surface current distribution at the resonance frequency is studied to further illustrate the mechanism of its stability. Finally, a prototype is fabricated and tested using the free-space method in an anechoic chamber, and the measured results agree well with the simulation. Due to its stable performance and beautiful appearance, the proposed FSS can be used in community communication.

REFERENCES

1. Ebrahimi, S. N., "Second-order terahertz bandpass frequency selective surface with miniaturized elements," *IEEE Transactions on Terahertz Science and Technology*, Vol. 5, No. 5, 761–769, Sept. 2015.

2. Monorchio, A., "A frequency selective radome with wideband absorbing properties," *IEEE Transactions on Antennas and Propagation*, Vol. 60, No. 6, 2740–2747, Apr. 2012.

3. Syed, I. S. and Y. Ranga, "A single-layer frequency-selective surface for ultra-wideband electromagnetic shielding," *IEEE Transactions on Electromagnetic Compatibility*, Vol. 56, No. 6, 404–1411, Dec. 2014.

4. Abadi, S. M. A. M. H. and N. Behdad, "Wideband linear-to-circular polarization converters based on miniaturized-element frequency selective surfaces," *IEEE Transactions on Antennas and Propagation*, Vol. 64, No. 2, 525–534, Feb. 2016.

5. Munk, B. A., P. Munk, and J. Pryor, "On designing Jaumann and circuit analog absorbers (CA absorbers) for oblique angle of incidence," *IEEE Transactions on Antennas and Propagation*, Vol. 55, No. 1, 186–193, Jan. 2007.

6. Allen, K. W., D. J. P. Dykes, D. R. Reid, and R. T. Lee, "Multi-Objective genetic algorithm optimization of frequency selective metasurfaces to engineer Ku-passband filter responses," *Progress In Electromagnetics Research*, Vol. 167, 19–30, 2020.

7. Pelton, E. and B. Munk, "A streamlined metallic radome," *IEEE Transactions on Antennas and Propagation*, Vol. 22, No. 6, 799–803, 1974.

8. Magill, E. and H. Wheeler, "Wide-angle impedance matching of a planar array antenna by a dielectric sheet," *IEEE Transactions on Antennas and Propagation*, Vol. 14, No. 1, 49–53, 1966.

9. Yin, W., H. Zhang, T. Zhong, and Q. Chen, "An outstanding miniaturized frequency selective surface based on convoluted interwoven element," *Progress In Electromagnetics Research Letters*, Vol. 69, 133–139, 2017.

10. Liu, H. L., K. L. Ford, and R. J. Langley, "Design methodology for a miniaturized frequency selective surface using lumped reactive components," *IEEE Transactions on Antennas and Propagation*, Vol. 57, No. 9, 2732–2738, Jul. 2009.

11. Yu, Y.-M., C.-N. Chiu, Y.-P. Chiou, and T.-L. Wu, "A novel 2.5-dimensional ultraminiaturized-element frequency selective surface," *IEEE Transactions on Antennas and Propagation*, Vol. 62, No. 7, 3657–3663, Jul. 2014.

12. Yu, Y., Z. Shen, T. Deng, and G. Luo, "3-D frequency-selective absorber with wide upper absorption band," *IEEE Transactions on Antennas and Propagation*, Vol. 65, No. 8, 4363–4367, Aug. 2017.

13. Rashid, A. K., B. Li, and Z. Shen, "An overview of three-dimensional frequency-selective structures," *IEEE Antennas and Propagation Magazine*, Vol. 56, No. 3, 43–67, Jun. 2014.

14. Li, B. and Z. Shen, "Dual-band bandpass frequency-selective structures with arbitrary band ratios," *IEEE Transactions on Antennas and Propagation*, Vol. 62, No. 11, 5504–5512, Nov. 2014.

15. Yin, W., H. Zhang, T. Zhong, and X. Min, "Ultra-miniaturized low-profile angularly-stable frequency selective surface design," *IEEE Transactions on Electromagnetic Compatibility*, Vol. 61, No. 4, 1234–1238, Aug. 2019.